Core Formation in *Escherichia coli* Bacterioferritin Requires a Functional Ferroxidase Center†

Suzanne Baaghil,‡ Allison Lewin,‡ Geoffrey R. Moore,* and Nick E. Le Brun*

Center for Metalloprotein Spectroscopy and Biology, School of Chemical Sciences and Pharmacy, University of East Anglia, Norwich NR4 7TJ, United Kingdom

Received July 16, 2003; Revised Manuscript Received September 24, 2003

ABSTRACT: Bacterioferritin from *Escherichia coli* is able to accumulate large quantities of iron in the form of an inorganic iron(III) mineral core. Core formation in the wild-type protein and a number of ferroxidase center variants was studied to determine key features of the core formation process and, in particular, the role played by the ferroxidase center. Core formation rates were found to be iron(II)-dependent and also depended on the amount of iron already present in the core, indicating the importance of the core surface in the mineralization reaction. Core formation was also found to be pH-dependent in terms of both rate and iron-loading characteristics, occurring with maximum efficiency at pH 6.5. Even at this optimum pH, however, the effective iron capacity was ∼2700 per molecule, i.e., well below the theoretical limit of ∼4500, suggesting that competing oxidation/precipitation processes have a major influence on the amount of iron accumulated. Disruption of the ferroxidase center, by site-directed mutagenesis or by chemical inhibition with zinc(II), had a profound effect on core formation. Effective iron capacities were found to be linked to iron(II) oxidation rates, and in zinc(II)-inhibited wild-type and E18A bacterioferritins core formation was severely restricted. Zinc(II) was also able, even at low stoichiometries (12−60 ions/protein), to significantly inhibit further core formation in protein already containing a substantial core, indicating the importance of the ferroxidase center throughout the core formation process. A mechanism is proposed that incorporates essential roles for the core surface and the ferroxidase center. A central feature of this mechanism is that dioxygen cannot readily gain access to the core, perhaps because the channels through the bacterioferritin coat are hydrophilic and dioxygen is nonpolar.

Ferritins comprise a widespread family of proteins that function in iron storage and detoxification (*1*−*5*). This is achieved through the formation of an iron(III)-containing mineral phase which is solubilized within the hollow center of the protein. The mechanism by which iron core formation occurs in these proteins is the subject of considerable interest. Our studies have focused on bacterioferritin from *Escherichia coli* (EcBFR),[1] which is composed of 24 identical 18.5 kDa subunits that pack to form the characteristic hollow, approximately spherical protein coat (*6*, *7*). The mineral cores of native bacterioferritins are generally phosphate-rich (*8*, *9*), though like other ferritins phosphate is not essential for core formation to occur. Uniquely among ferritins, BFRs contain up to 12 heme groups, which are situated between symmetry-related subunit pairs (*6*, *10*, *11*), (Figure 1), though these groups do not play a role in aerobic uptake of iron(II) (*11*). Each subunit contains a dinuclear metal-binding site in which each metal ion is capped by carboxylate and histidine ligands and connected to the other metal by two bridging carboxylate groups (*5*, *6*, *12*, *13*). This center (known as the ferroxidase center) plays a key role in the early stages of iron uptake into the protein (*12*, *13*), which consists of three distinct kinetic phases: binding of two iron(II) ions per dinuclear center (phase 1), rapid oxidation of the iron(II) ions to iron(III) in the presence of dioxygen (phase 2), and subsequent core formation (phase 3). The latter is only observed when more than two iron(II) ions per subunit are added (*12*).

Previously we showed that replacement of a single ferroxidase center glutamate residue results in the loss of the phase 2 reaction and a dramatic decrease in the rate of phase 3 (*13*). However, since iron(II) oxidation was still observed, it was concluded that core formation could occur by a mechanism independent of the ferroxidase center. This was consistent with the proposed mechanism of core formation in mammalian ferritins, in which oxidation of iron(II), under conditions of high iron flux, occurs at the growing core surface following nucleation of the core (*15*−*19*).

Using spectrophotometric methods and employing copper(II) and zinc(II) as mechanistic probes, we have investigated the phase 3 core formation reaction to saturation in wild-type and ferroxidase center variants of EcBFR. We demonstrate that the rate of core formation and the ability of the

† This work was supported by a grant from the U.K. Biotechnology and Biological Sciences Research Council, Grant ref 83/B14704.

* Corresponding authors. G.R.M.: fax +44 1603 592697; e-mail g.moore@uea.ac.uk. N.L.B.: fax +44 1603 592003; e-mail n.le-brun@uea.ac.uk.

‡ These authors contributed equally to the work.

[1] Abbreviations: EcBFR, *Escherichia coli* bacterioferritin; IPTG, isopropyl β-D-thiogalactopyranoside; HEPES, 4-(2-hydroxyethyl)piperazine-1-ethanesulfonic acid; HuHF, human H-chain ferritin; MES, 2-(*N*-morpholino)ethanesulfonic acid; PAGE, polyacrylamide gel electrophoresis; PCR, polymerase chain reaction; SDS, sodium dodecyl sulfate.

10.1021/bi035253u CCC: $25.00 © 2003 American Chemical Society
Published on Web 10/29/2003

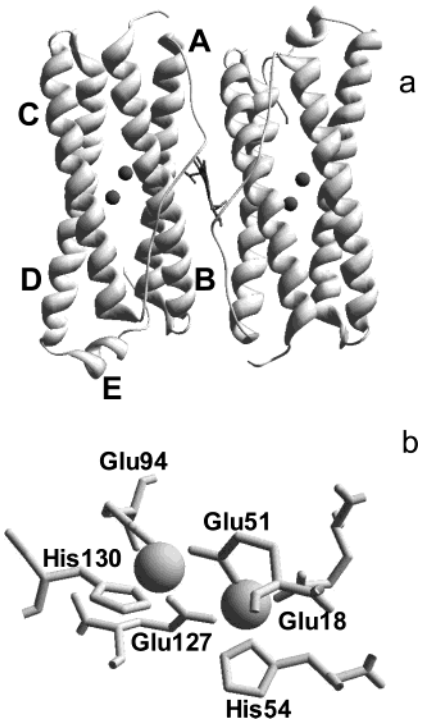

FIGURE 1: EcBFR subunit dimer and ferroxidase center: Schematic representations of (a) the EcBFR subunit dimer, showing the intersubunit location of the b-type heme group and the intrasubunit ferroxidase center, and (b) the ferroxidase center. The ligands to the ferroxidase center are located on helices A−D: helix A, Glu18; helix B, Glu51 and His54; helix C, Glu94; helix D, Glu127 and His130. The figures were generated by Swiss PDB Viewer 3.7b2 (*14*) with the BFR coordinates.

cavity to accumulate iron are pH-dependent, and under the conditions tested, a maximum of ~2700 irons could be accommodated per protein, yielding a core that is charge-neutral. We show that the ferroxidase center variants E127Q, H130E, and E18A EcBFR have significantly reduced abilities to store iron and that this is correlated to decreases in their iron(II) oxidation activities. Zinc(II), a ferroxidase center inhibitor (*13*, *20*, *21*), severely reduces the ability of the wild-type protein to oxidize and store iron, even when added to EcBFR already containing an iron core. These data combined indicate that the ferroxidase center is involved in catalysis throughout core formation and not only in core nucleation. This and previous data lead to a proposal for the mechanism of core formation that accounts for the roles of the ferroxidase center and the core surface in core formation and gives important new insight into the key differences between mineralization processes in BFR and mammalian ferritins.

MATERIALS AND METHODS

E18A EcBFR was generated by two-stage PCR with the wild-type *bfr* gene (in pGS758) as a template and reverse and CCGCCATGGCTCAACCTTCTTCG as flanking primers. The latter was used to introduce an *Nco*I site (underlined) downstream of the *bfr* gene. GATTGCGACAAGCGCATTTCCCAACAG was used as mutagenic primer. The fragment encoding E18A was ligated into *Sma*I-cut pUC18, generating pLBN2, and the *Nde*I/*Nco*I fragment was subsequently ligated into pAlter-Ex1 (containing a functional ampicillin resistance cassette) cut with the same enzymes, giving pLBN4. E127Q and H130E EcBFRs were generated by a whole-plasmid mutagenesis method, as previously described (*22*). The primers ATTTTGCGTGATCAAGAAGGCCATATC and GATGAAGAAGGCGAGATCGACTGGCTG together with their reverse complements were used with pGS758 as template to generate the E127Q and H130E mutations, respectively, giving pALN2 (E127Q) and pALN3 (H130E). The *Nde*I/*Eco*RI fragment (containing the mutated *bfr* gene) from each of these plasmids was ligated into pET21a cut with the same enzymes to give pALN5 (E127Q) and pALN6 (H130E). The mutant constructs were confirmed by sequencing.

For pLBN4 in host *E. coli* JRG2157 (JM101 *bfr*$^-$), preliminary experiments showed that *bfr* expression occurred to the same extent in the absence or presence of the inducer IPTG, and so this was omitted from subsequent cultures. For pALN5 and pALN6 in *E. coli* AL1 [BL21(DE3) *bfr*$^-$], cultures were induced with IPTG (1 mM final concentration) when $A_{650nm} = 0.8-0.9$. In all cases, BFR was purified as previously described (*23*).

Iron oxidation measurements were made on a Perkin-Elmer λ35 or λ800 spectrophotometer. Iron(II) was added to apo-BFR as ferrous ammonium sulfate, freshly prepared by dissolving weighed amounts of the salt in deoxygenated water. The addition of 0.25 mL of concentrated HCl/100 mL of solution was found to stabilize iron(II) against autoxidation. Solutions of copper(II) chloride and zinc(II) sulfate were prepared by dissolving weighed amounts of the salts in water. The water and salts used were all analytical grade. Microliter additions of metal ion solutions were made with a microsyringe (Hamilton). For experiments involving the addition of two or more different metal ions, samples were incubated for 5 min between additions, except for iron(II), for which oxidation was allowed to go to completion before further additions were made. Following completion of oxidation, as judged from a constant A_{340nm} value, samples were centrifuged at 10 000 rpm for 5 min to remove any iron(III) precipitate not associated with the protein, prior to subsequent additions. Protein precipitation was detected through a large decrease in absorbance in the near-UV region following centrifugation. In several instances, this was confirmed by analysis of the protein content of the precipitate and supernatant, which indicated ~90% precipitation.

Extinction coefficients (as per iron values) at 340 nm for iron-BFR species were determined by two methods. First, they were calculated directly from UV−visible absorbance difference spectra resulting from the addition of 400 iron(II) ions to apo-EcBFR samples, making the assumption that all iron added was incorporated into the protein. Second, the iron content of iron-EcBFR samples (at different points in the titration) was determined by iron analysis (*24*) following passage of the sample down a Sephadex G25 column. ϵ_{340nm} values were then calculated by reference to postcolumn absorbance spectra. The two methods gave values in good agreement.

Rates of phase 3 iron(II) oxidation were calculated from initial, linear increases in A_{340nm} per unit time. Because ϵ_{340nm} values were not constant between samples, values of ΔA_{340nm} s^{-1} were converted to iron(II) oxidized per second (μM s^{-1}).

Protein concentrations were determined by the bicinchoninic acid method with bovine serum albumin as a standard (*25*) or spectrophotometrically by use of $\epsilon_{280nm} = 33\,000$ M^{-1} cm^{-1} subunit (*21*). Heme concentrations were determined

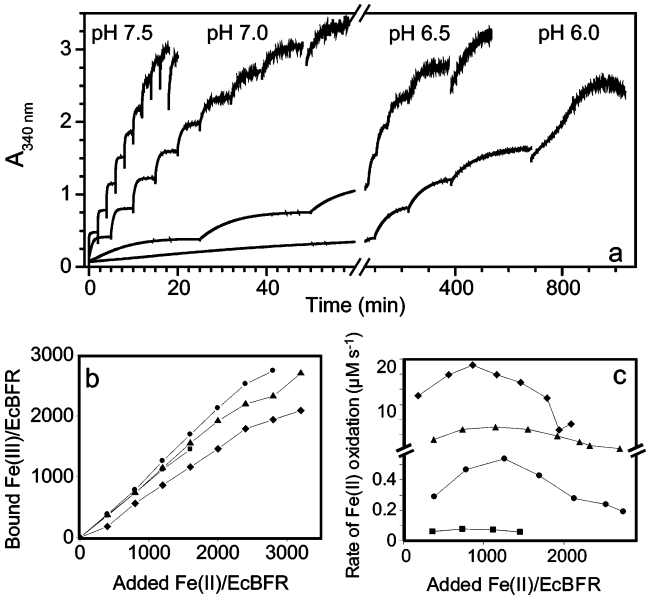

FIGURE 2: EcBFR-catalyzed iron core formation as a function of pH. (a) Absorbance increases at 340 nm as a function of time following additions of 400 iron(II)/EcBFR molecule. Following completion of oxidation, each sample was centrifuged to remove any precipitated iron, as described under Materials and Methods. EcBFR (0.5 μM) was in 0.1 M MES for pH values 6.0 and 6.5 and in 0.1 M HEPES for pH values 7.0 and 7.5. Temperature was 25 °C and path length was 1 cm. The increased noise observed at high iron loadings is caused by a combination of decreasing transmitted light and precipitation of the samples. (b) For the titrations in panel a, the average number of bound iron(III) ions per molecule is plotted against iron(II) added: ■, pH 6.0; ●, pH 6.5; ▲, pH 7.0; ◆, pH 7.5. (c) Plots of rates of iron(II) oxidation (calculated as described under Materials and Methods from the data in panel a) as a function of iron(III) bound per protein. The bound iron values correspond to the total iron(III) bound following the indicated addition, and the corresponding rate refers to the initial rate for that addition. Symbols used are as in panel b.

by the pyridine hemochromogen method of Falk (*26*) and were found to be 1, 8, 4, and 1.5 per protein for wild type, E18A, H130E, and E127Q EcBFR, respectively. Iron was removed from EcBFR by reduction with sodium dithionite and complexation with 2,2′-bipyridyl, as previously described (*27*). Anion-exchange chromatography of apo- and holo-wild-type EcBFR was carried out on a 5 mL HiTrap Q HP column (Amersham Biosciences) equilibrated in 0.1 M MES, pH 6.5. Proteins were eluted with a gradient of 0−0.5 M NaCl in the same buffer. The holo-EcBFR sample was generated by adding aerobically 2000 iron(II) ions/EcBFR molecule at 25 °C, and following completion of oxidation, passage of the sample down a Sephadex G-25 column. Native gel electrophoresis of apo- and holo-EcBFR samples was carried out by the Laemmli system (*28*) but with 7.5% acrylamide and no SDS.

RESULTS

pH Dependence of Phase 3 of EcBFR Iron Core Formation. Sequential additions of 400 iron(II) ions/molecule were made to EcBFR solutions and oxidation of the iron(II) to iron(III) was followed at 340 nm, as described under Materials and Methods, with the pH of the BFR solution varied between 6.0 and 7.5. Figure 2a shows measurements for EcBFR at pH 6.0, 6.5, 7.0, and 7.5. Precipitation of the protein samples was observed at different points in the titrations, revealing a pH dependence of the ability of EcBFR to accumulate iron. Thus, precipitation was observed after addition of five aliquots of iron (2000 iron(II) ions/EcBFR) at pH 6.0 and after nine aliquots (3600 irons/EcBFR) at pH 7.0.

Effective iron capacities (i.e., the maximum number of iron ions that can be accommodated before precipitation occurs under defined conditions) could not be determined from the amount of iron(II) added alone because the inclusion of a centrifugation step following the completion of oxidation showed that, in some cases and particularly at the higher pH values studied, not all of the oxidized iron was solubilized by the protein. Therefore, quantities of iron(III) associated with the protein after each iron(II) addition were determined directly by iron analysis as described under Materials and Methods; see Figure 2b. Effective iron capacities were pH-dependent: at pH 6.0 only an average of ∼1450 iron(III) ions could be accommodated in the EcBFR core before precipitation occurred. Effective capacity increased up to ∼2700 iron(III)/EcBFR at pH 6.5−7.0, after which it decreased again (see Table 1). Figure 2b shows that EcBFR core formation is most efficient at pH 6.5, in terms of the proportion of iron added that is stored and the effective capacity. Extinction coefficients at 340 nm (ϵ_{340} values) were determined with reference to the concentration of stored iron-(III) [i.e., as per iron(III) quantities]; see Table 1. These show that the optical properties of the iron(III) mineral core are also dependent on the pH of the solution in which they are formed. The optical properties of cores formed at pH 6.0 and 7.5 were not affected by subsequently changing the pH, indicating that the different cores could not be reversibly interconverted.

The rate of EcBFR core formation is pH-dependent, as expected for a reaction that results in the release of two protons for each iron(II) oxidized/hydrolyzed (*21*). Rates of iron(II) oxidation [in units of micromolar iron(II) oxidized per second] were plotted as a function of iron(III) ions bound per BFR molecule;[2] see Figure 2c. Rates measured at pH 6.5 are in good agreement with previous measurements (*23*). As expected, rate increased with pH. Interestingly, all of the plots of rate of iron(II) oxidation versus amount of iron(III) bound to BFR had a similar form: rates increased up to 800−1200 iron(III)/protein and then subsequently decreased to the point at which precipitation occurred. As a control, iron(II) autoxidation (i.e., in the absence of EcBFR) was measured (from the increase in absorbance at 340 nm with time) at each pH value (data not shown) and rates were calculated;[3] see Table 1. These were significantly lower than rates observed in equivalent EcBFR experiments, and in each case, a precipitate of iron(III) hydroxide was formed.

In the above experiments, iron(II) was added to EcBFR in aliquots of 400/molecule. To investigate how the amount

[2] Iron per protein is in the form of iron(III) bound per protein rather than iron(II) added per protein, because not all of the added iron is assimilated into the protein core.

[3] A_{340nm} traces resulting from the autoxidation of iron(II) are complex, presumably due to a dependence of the rate on the presence of precipitated iron(III) mineral. For the rate calculations, we have examined the time frame relevant to the BFR experiment, i.e., BFR core formation takes place over a period of approximately 100 min at pH 6.0 and so the first 100 min of the pH 6 autoxidation trace were analyzed.

Table 1: Summary of Iron Core Formation Data for Wild-Type BFR and Ferroxidase Center Variants

	wt BFR, pH 6.0	wt BFR, pH 6.5	wt BFR, pH 7.0	wt BFR, pH 7.5	E18A, pH 6.5	E127Q, pH 6.5	H130E, pH 6.5
rate of iron(II) oxidation (μM s^{-1})[a]							
first addition	0.060 ± 0.001	0.29 ± 0.01	3.10 ± 0.09	12.3 ± 0.2	0.004 ± 0.001	0.13 ± 0.01	0.036 ± 0.002
pre-precipitation addition	0.056 ± 0.002	0.19 ± 0.01	1.29 ± 0.09	6.4 ± 0.2	0.004 ± 0.001	0.083 ± 0.005	0.044 ± 0.002
maximum	0.077 ± 0.001	0.54 ± 0.01	5.75 ± 0.02	18.7 ± 0.4	0.004 ± 0.001	0.167 ± 0.007	0.044 ± 0.002
$\epsilon_{340\ nm}$ per iron(III) (M^{-1} cm^{-1})	1955 ± 15	1775 ± 15	1950 ± 60	2285 ± 55	1870 ± 60	1900 ± 150	2010 ± 50
maximum iron(III) bound per BFR	~1450	~2700	~2700	~2000	~335[b]	~1200	~700
			BFR-free control				
rate of iron(II) oxidation (μM s^{-1})	0.002 ± 0.0005	0.008 ± 0.001	0.60 ± 0.01	2.4 ± 0.1			

[a] Rates of iron(II) oxidation and maximum iron(III) bound per protein molecule were calculated as described under Materials and Methods. All measurements were conducted at 200 μM iron(II). [b] When iron(II) was added in aliquots of 50/protein (equivalent to 25 μM), only ~130 iron(III)/protein were accumulated.

of iron(II) added per aliquot affects the core formation process, similar experiments were performed at pH 6.5 with aliquots of 200 and 800 iron(II)/molecule (not shown). The rate of iron(II) oxidation for the first aliquot showed a first-order dependence on iron(II) [for subsequent additions, rates continued to show an iron(II) dependence, although the form of this was not clear because, following the first addition, samples were no longer equivalent]. Interestingly, it was recently shown that the rate of mineralization in human H-chain ferritin (HuHF) is not iron-dependent; initial rates measured for different iron additions were the same, leading to the conclusion that all iron(II) oxidation during the early part of core formation occurs via the ferroxidase center (*19*). The form of the plots from the 200 and 800 iron(II)/BFR experiments was similar to that of the 400 iron(II) experiment; rates increased before tailing off toward the point of precipitation. For the 200 iron(II) aliquot experiment, the rate maximum was at ~800−1200 iron(III)/protein (i.e., similar to the 400 iron(II) experiment), while for the 800 iron(II) aliquot experiment, the maximum appeared to be at ~1550 iron(III) ions, but the nature of the experiment means that there are insufficient data points to conclude that there is a significant difference. The effective iron capacities of the core were very similar at ~2700. Thus, apart from the expected rate dependence, the core formation process is not dependent on the size of the iron(II) aliquots employed to build up the core.

Net Electrostatic Properties of the EcBFR Core. The formation of an iron core containing large numbers of iron(III) ions should lead to changes in the electrostatic characteristics of the protein unless these ions are charge-balanced by anions such as hydroxide and oxide. To investigate this, apo-EcBFR and EcBFR following the aerobic addition of 2000 iron(II) ions per molecule (in aliquots of 400) at pH 6.5 were analyzed by anion-exchange chromatography. Figure 3 shows the elution profile (detected via A_{280}) as a function of the salt concentration. This shows clearly that the presence of the core does not influence the net electrostatic properties of the protein. This was confirmed by native PAGE analysis (not shown), which showed that the electrophoretic properties of BFR are unaffected by the presence of an iron core.

Inactivation of the Ferroxidase Center by Site-Directed Mutagenesis. From previous studies of variants of EcBFR containing substitutions of ferroxidase center residues, it was concluded that the ferroxidase center is essential for core formation to occur at the wild-type rate but that core formation still occurs in the absence of a fully functional

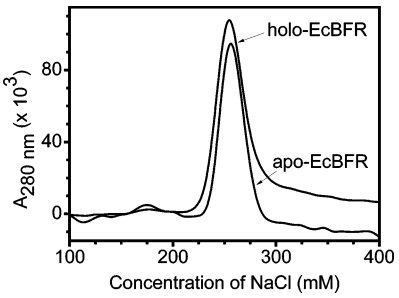

FIGURE 3: Anion-exchange chromatographic properties of apo- and holo-EcBFR: Chromatogram showing elution profiles (A_{280nm} as a function of NaCl concentration) of apo-EcBFR and holo-EcBFR (see text for details). EcBFR (precolumn concentration 3.6 μM) was in 0.1 M MES, pH 6.5. Holo-EcBFR absorbance intensities were normalized to those of apo-EcBFR to aid comparison between the two samples.

center (*13*). This was based on the addition of a single aliquot of 400 iron(II)/BFR, and so a more thorough investigation of BFR variants containing substitutions at the ferroxidase center was conducted. The selection of BFR variants was based on rates of iron oxidation: by studying variant proteins with different activities, we hoped to gain insight into the core formation process and, in particular, the factors controlling core formation rates and effective iron capacities. E18A, E127Q, and H130E EcBFRs all showed, to varying degrees, decreased iron(II) oxidation activity relative to wild type (see below).

Sequential additions of 400 iron(II) ions/BFR were made to samples of E127Q, H130E, and E18A EcBFR, and absorbance at 340 nm was monitored (Figure 4a). The first addition to E18A EcBFR resulted in a trace very similar to that previously reported (*13*), except that oxidation was followed up to ~800 min where it was essentially complete. For E127Q, H130E, and E18A EcBFR, precipitation occurred after addition of 1600, 1200, and 800 irons, respectively, of which ~1200, ~700, and ~335 were found to be bound to BFR as iron(III) immediately prior to precipitation. Rates of iron(II) oxidation were plotted as a function of iron(III) bound (Figure 4b). With the exception of E18A EcBFR, oxidation rates increased after the first addition, passed through a maximum, and subsequently decreased, as observed for wild-type EcBFR. The maximum rate occurred at 700−800 iron(III) for E127Q and H130E EcBFR, which is different from the wild-type protein [~1200 iron(III)]. In the case of H130E EcBFR, precipitation was observed immediately after the rate maximum was reached. The rate of oxidation in E18A EcBFR (Figure 4b and Table 1) was

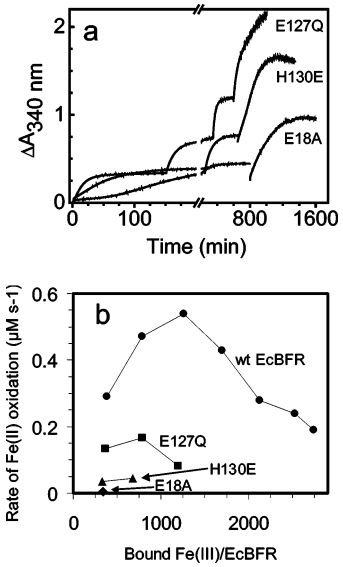

FIGURE 4: Core formation in EcBFR ferroxidase center variants. (a) Absorbance increases at 340 nm as a function of time following additions of 400 iron(II)/EcBFR molecule to E127Q, H130E, and E18A EcBFRs. Samples were treated as described in Figure 2a. BFRs (0.5 μM) were in 0.1 M MES, pH 6.5. Temperature was 25 °C and path length was 1 cm. (b) Plots of rates of iron(II) oxidation (calculated from the data in panel a) as a function of iron(III) bound per protein. Wild-type rates are added to aid comparison. (●) Wild type, (■) E127Q, (▲) H130E, and (◆) E18A EcBFRs are shown.

lower than that of autoxidation under similar conditions, indicating that the protein, rather than catalyzing iron(II) oxidation, actually stabilizes iron(II) against oxidation.

To obtain a more detailed picture of events, the E18A EcBFR experiment was repeated with aliquots of 50 iron(II) ions per molecule. Figure 5a shows absorbance at 340 nm as a function of time for sequential additions of iron(II). Precipitation of the protein was observed following the addition of 200−250 iron(II) ions, and analysis of the capacity of the core for iron under these conditions showed that a maximum of only ∼130 iron(III)/protein could be accommodated before precipitation was observed. Thus E18A BFR is severely restricted in its ability to lay down an iron core.

Inactivation of the Ferroxidase Center by Inhibition with Zinc(II). It has been previously demonstrated that zinc(II) binds at the ferroxidase center with a higher affinity than iron(II) and is able to effectively block the center, preventing it from catalyzing iron(II) oxidation (*13*, *20*, *21*). Thus, in the presence of two zinc(II) ions per subunit, phases 1 and 2 of core formation do not occur. Iron(II) oxidation is, however, observed (albeit at a very low rate), and so there remains the possibility that an iron core is formed. To compare the activities of E18A EcBFR with those of zinc(II)-EcBFR, wild-type EcBFR containing 48 zinc(II) ions per molecule was titrated with aliquots of 400 (data not shown) and 50 iron(II) (Figure 5a). Precipitation was observed after addition of the third [1200 iron(II)/protein] and sixth [300 iron(II)/protein] aliquots for the 400 and 50 iron experiments, respectively, of which ∼550 and ∼170 were found associated with the protein as iron(III) immediately before precipitation. Rates for the 50 iron experiment are plotted as a function of iron(III) bound along with those for E18A EcBFR; see Figure 5b. Similar, very low rates were observed for both EcE18A and Zn(II)-inhibited

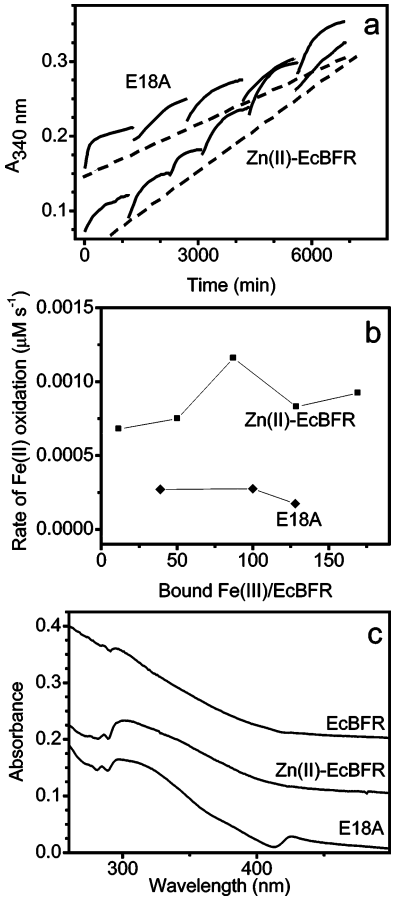

FIGURE 5: Effect on core formation of ferroxidase center inactivation by mutagenesis and zinc(II) inhibition. (a) Absorbance increases at 340 nm as a function of time following additions of 50 iron(II)/EcBFR molecule to E18A EcBFR alone and wild-type BFR containing 48 zinc(II) ions/protein. Samples were treated as described in Figure 2a. EcBFRs (0.5 μM) were in 0.1 M MES, pH 6.5. Temperature was 25 °C and path length was 1 cm. (b) Plot of rates of iron(II) oxidation (calculated from the data in panel a) as a function of iron(III) bound per protein: (■) zinc(II)-EcBFR; (◆) E18A EcBFR. (c) UV−visible difference absorbance spectra of iron(III) core species formed in E18A EcBFR and Zn(II)-EcBFR following the addition of the third iron aliquot in panel a. An equivalent spectrum resulting from the addition of 150 iron(II) ions to wild-type BFR in aliquots of 50 is also shown for comparison. Conditions were as described for panel a. The spectra for zinc(II)-EcBFR and wild-type EcBFR are offset by +0.1 and +0.2 absorbance unit, respectively, to allow comparison. Spectra of the corresponding apoproteins were used to generate the difference spectra.

BFR. Thus, occupation of the ferroxidase center by zinc(II) severely restricts the ability of BFR to form an iron core, such that the protein behaves in a similar way to BFR containing a mutated, nonfunctional ferroxidase center. These data are consistent with the conclusion that a functional ferroxidase center is required for phase 3 core formation.

Optical Properties of Iron(III) in the Presence and Absence of a Functional Ferroxidase Center. The UV−visible spectrum of the wild-type BFR iron(III) core, due to O → Fe(III) charge-transfer transitions, had an intensity maximum in the UV and a tail that extended well out into the visible. A small shoulder on the absorbance envelope was observed at 300 nm. In the absence of a functional ferroxidase center, similar values for ϵ_{340} were observed (see Table 1), but measurements in the range 260−500 nm revealed significant differences in the spectra. Figure 5c shows difference spectra

following the addition of 150 iron(II)/EcBFR (in aliquots of 50) to E18A, zinc(II)-EcBFR, and wild-type EcBFR. Spectra for E18A and zinc(II)-EcBFR contained a much more pronounced shoulder at ~300 nm.[4] Measurement of the spectrum arising from the autoxidation of iron(II) in 0.1 M MES buffer at pH 6.5 revealed a distinct peak at 300 nm (not shown). The similarity in the spectral features arising from the core formed in E18A and zinc(II)-inhibited EcBFR with those of the iron(III) product of iron(II) autoxidation indicates that these small cores are structurally distinct from the early wild-type core.

Zinc(II) Inhibition of Core Formation in Wild-Type BFR Containing an Established Iron Core. That BFR core formation essentially does not occur in the absence of a functional ferroxidase center raises the question of what role the center plays in core formation. This was investigated further through studies of the effect of zinc(II) at later stages of core formation. Iron(II) ions were added at pH 6.5 (800 or 1200/EcBFR, in aliquots of 400), with each addition being allowed to completely oxidize and any precipitated iron removed prior to the subsequent addition of further iron. To separate samples of holo-EcBFR containing, on average, 800 or 1200 irons/molecule,[5] 0, 12, 24, 48, and 60 zinc(II) ions were added per molecule, followed by the resumption of iron(II) additions. Rates of iron(II) oxidation and the quantities of iron(III) associated with the protein following oxidation were determined for each addition, and the data for 800 and 1200 irons are plotted in Figure 6, panels a and b, respectively. Major differences were observed in rates and effective iron capacities following the additions of zinc(II). After the addition of zinc(II), the proportion of the iron added that remained associated with the protein decreased significantly; e.g., in the 1200 iron core experiment, at 24 zinc(II)/protein, very little additional iron could be added to the core before precipitation occurred. The effect of zinc(II) on oxidation rates for the first addition of iron(II) following the addition of zinc(II) is shown for both 800 and 1200 iron experiments in Figure 6c. This shows that the addition of 12 zinc(II) ions per molecule decreased the rate of iron(II) oxidation by approximately a half [relative to that measured in the absence of zinc(II)], and that 24, 48, and 60 zinc(II) ions resulted in further decreases, down to less than a fourth that of the zero zinc control. Thus, zinc(II), even at very low levels relative to iron, is able to inhibit core formation. The fact that the two plots in Figure 6c are very similar indicates that the effect of zinc(II) is not dependent on the size of the core.

Restoration of Ferroxidase Activity in Ferroxidase Center-Deficient EcBFR by Copper(II). Previously, it has been demonstrated that addition of copper(II) enhances the rate of core formation in wild-type EcBFR and that the effect of

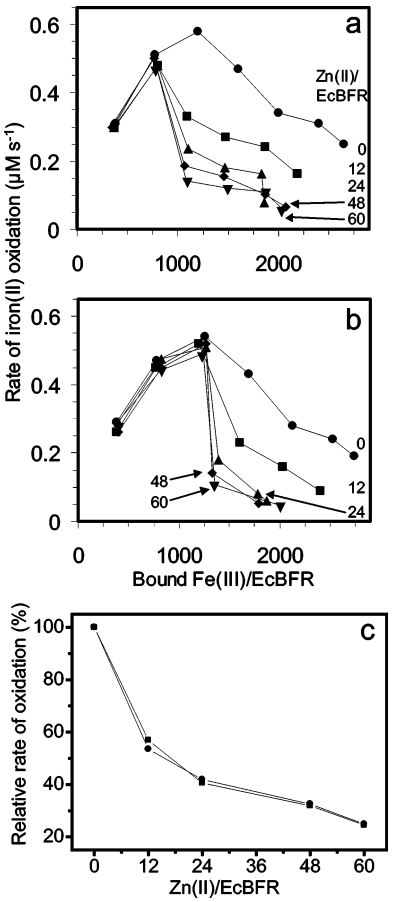

FIGURE 6: Zinc(II) inhibition of core formation in EcBFR already containing a core. (a) Plots of rates of iron(II) oxidation as a function of the average number of iron(III) bound per EcBFR. Iron(II) was added in aliquots of 400/protein, and after the addition of 800 iron(II) ions, varying amounts of zinc(II) were added per protein as indicated before the resumption of iron(II) additions: (●) zero zinc(II) control; (■) 12 zinc(II); (▲) 24 zinc(II); (◆) 48 zinc(II); (▼) 60 zinc(II). EcBFR (0.5 μM) was in 0.1 M MES, pH 6.5. Temperature was 25 °C. (b) As in panel a except that zinc(II) was added after the addition of a total of 1200 iron(II)/protein. (c) Plots of the relative rates of iron(II) oxidation for the first iron addition following addition of zinc(II) to EcBFR containing ~800 and ~1200 iron(III)/molecule, as a function of zinc(II) added per protein. Here, the zero zinc(II) control is set to 100%. (■, ●) 800 and 1200 iron core experiments, respectively.

copper is associated with the protein, but independent of the ferroxidase center (*23*). It was also shown that copper(II) can restore iron(II)-oxidation activity to zinc(II)-inhibited EcBFR, consistent with the effect of copper(II) being independent of the ferroxidase center. We investigated the proposal that copper(II) should also be able to restore iron(II) oxidation activity in E18A EcBFR. Figure 7 shows the effect of the addition of 48 copper(II) ions per E18A EcBFR on the oxidation of iron(II) (added in 400 iron aliquots) as observed through increases in absorbance at 340 nm. Rates of oxidation as a function of iron(III) associated with the protein were plotted; see Figure 7b. For the first three aliquots of iron(II) added, rates of iron(II) oxidation were restored to a level similar to that observed for wild-type BFR. The plot had a similar form to that of wild-type BFR in that it passed through a maximum, but this was observed at ~800 iron(III)/molecule rather than ~1200 as it was for wild-type BFR. Analysis of the effective capacity of the E18A EcBFR core in the presence of copper showed that it could

[4] The intensities are consistent with the relative accumulations of iron(II) within the proteins at this point during the titration: E18A, Zn(II)-BFR, and wild-type BFR contain ~125, ~75, and ~150 iron(III)/protein. The feature at ~420 nm is due to a small perturbation of the heme Soret band upon iron uptake. This is observed in E18A BFR and not in wild-type BFR because of the much higher heme content in the former.

[5] Evidence from electron microscopic studies of BFR cores containing on average 400 and 2000 iron(III) ions, prepared as described here (Li, Baaghil, Le Brun, Moore, and Mann, unpublished data), indicated a distribution of core sizes similar to that previously reported for BFRs and mammalian ferritins (*29*).

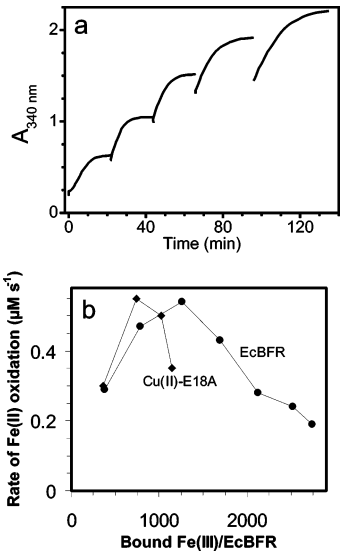

FIGURE 7: Copper(II)-enhanced core formation in E18A EcBFR. (a) Absorbance increases at 340 nm as a function of time following additions of 400 iron(II)/BFR molecule to E18A EcBFR containing 48 copper(II) ions/protein. Samples were treated as described in Figure 2a. E18A EcBFR (0.5 μM) was in 0.1 M MES, pH 6.5. Temperature was 25 °C and path length was 1 cm. (b) Plot of rates of iron(II) oxidation (calculated for E18A EcBFR from the data in panel a and for wild-type EcBFR from Figure 2a) as a function of iron(III) bound per protein. (●, ◆) Wild-type and E18A EcBFR, respectively.

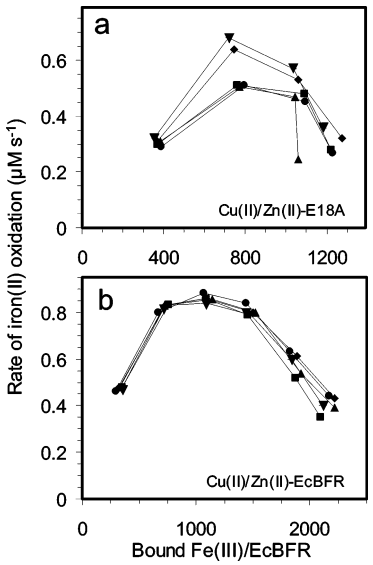

FIGURE 8: Effect of copper(II) on zinc(II) inhibition of core formation in BFR containing a core. (a) Plots of rates of iron(II) oxidation as a function of the average number of iron(III) bound per E18A EcBFR molecule. Iron(II) was added to E18A EcBFR containing 48 copper(II) ions/protein in aliquots of 400/protein. After the first aliquot, varying amounts of zinc(II) were added per protein, as indicated, before the resumption of iron(II) additions: (■) zero zinc(II) control; (●) 12 zinc(II); (▲) 24 zinc(II); (◆) 48 zinc(II); (▼) 60 zinc(II). E18A EcBFR (0.5 μM) was in 0.1 M MES, pH 6.5. Temperature was 25 °C. (b) As in panel a except that wild-type EcBFR was used.

accommodate on average ~1200 iron(III) ions. Difference spectra measured over the range 260−500 nm (not shown) showed that the mineral initially gave absorbance similar to that of wild-type EcBFR but that a shoulder similar to that observed at 300 nm for E18A EcBFR alone [and for zinc-(II)-EcBFR] became increasingly apparent at higher core iron levels. We note that for additions above 800 irons only a relatively low percentage of the added iron(II) became associated with the protein and precipitation occurred much earlier than in the wild-type case. We conclude that addition of copper(II) restores the ability of E18A EcBFR to lay down a sizable iron core but that it does not fully confer wild-type EcBFR core formation properties on the variant. The data support the proposal that core formation can occur provided that a catalytic center for iron(II) oxidation is associated with the protein.

Zinc(II) Does Not Inhibit Iron Core Formation in Copper-(II)-EcBFR or Copper(II)-E18A EcBFR Samples Containing Established Cores. To investigate the possibility that zinc-(II) inhibition of further core formation in BFR containing an established core arises from zinc(II) binding in the protein coat channels, through which iron(II) likely accesses the cavity, we expanded on previous work that showed that the addition of copper(II) to apo-EcBFR can overcome the inhibitory effect of zinc(II) (*23*). Forty-eight copper(II) ions were added to apo-E18A EcBFR and apo-EcBFR, followed by 400 iron(II) ions that were allowed to fully oxidize. Any precipitated iron was removed by centrifugation before separate additions of 0, 12, 24, 48, and 60 zinc(II) ions/molecule, followed by further iron(II) additions. Rates of iron(II) oxidation and the quantities of iron(III) associated with E18A EcBFR and wild-type BFR following oxidation were determined for each addition (Figure 8). No inhibitory effect of zinc(II) was observed in terms of the rate of core formation or in the amount of additional iron that could be incorporated. In fact, higher additions of zinc(II) resulted in a small enhancement of the rate of Fe(II) oxidation for E18A EcBFR. These data indicate that zinc(II) does not prevent iron(II) access to the cavity by binding in, and thereby blocking, the channels in the EcBFR protein coat.

DISCUSSION

In this paper we have shown that the rate of core formation and the effective capacity of the EcBFR core for accumulating iron are pH-dependent. Although core formation occurs much more rapidly at increasing pH, maximum efficiency in terms of the fraction of iron added that is sequestered by the protein and the maximum effective iron capacity was found at pH 6.5 (Figure 2). The form of plots of rate against iron(III) bound is similar at each pH value and is similar to that previously reported for BFR (*23*, *29*): the rate of core formation increases up to ~1200 iron(III)/protein and then gradually decreases to the point of saturation and precipitation. Similar observations have been made for mammalian ferritins, and these led to the proposal of the crystal growth mechanism, i.e., that the growing core surface is the site of oxidation of incoming iron(II) (*15*). The maximum rate corresponds to the protein cavity being half-filled because this represents the largest available surface area, and further growth of the core leads to a reduction in surface area. The data presented here are consistent with a role for the growing core surface in catalyzing iron(II) oxidation. The maximum iron capacity measured under the conditions tested was ~2700. This is significantly less than theoretical value of ~4500 (*30*, *31*) calculated for mammalian ferritin under the assumption that the crystalline core has a ferrihydrite-like structure (i.e., $5Fe_2O_3{\cdot}9H_2O$) (*32*−*34*) but significantly greater than the average iron content of BFR cores isolated

from nonoverxpressing strains (*2*). An effective capacity well under 4500 was also recently observed for horse spleen ferritin (*35*). This could indicate that the optimum conditions for core loading have not yet been found, and/or that the often-quoted theoretical maximum is an overestimation (e.g., it is unlikely that the ferrihydrite crystal form precisely describes the ferritin/BFR iron oxide mineral). Whatever the true theoretical maximum, we have also observed here, under different conditions, effective iron capacities much lower than ~2700, indicating that effective capacities are not determined by the physical limitations of the protein cavity. Thus, the EcBFR cavity likely has a theoretical capacity similar to that of mammalian ferritin, but a major factor in determining the point at which precipitation occurs is the balance between rates of core formation and noncore oxidation processes, including autoxidation. When core formation rates reduce to be within the range of autoxidation processes, then the latter will occur to an appreciable extent. Noncore oxidation may occur at other sites within the protein, for example, within the protein coat channels that provide access for iron(II) into the cavity (*36*, *37*). This would lead to a gradual blocking of iron(II) access routes, which would further promote extraprotein autoxidation reactions. Formation of an iron(III) precipitate in the reaction mixture rapidly leads to protein aggregation and precipitation. It is noteworthy that at the optimum pH for core formation (pH 6.5) the rates of BFR-catalyzed iron(II) oxidation and autoxidation are very different (Table 1). The exact composition and structure of the core are likely to be other important factors in determining the effective iron capacity. Variability in the optical properties of cores formed under different conditions (Figure 5b) implies that structural differences do exist.

A dependence of the effective iron capacity on how iron(II) was added was not observed for wild-type BFR but was for E18A EcBFR [capacities of ~335 and ~130 observed when iron(II) was added in aliquots of 400 and 50, respectively] and zinc(II)-EcBFR [capacities of ~550 and ~170 observed when iron(II) was added in aliquots of 400 and 50, respectively]. This is consistent with the above proposal because the variant proteins exhibit very low iron(II) oxidation and core formation activities, and so autoxidation processes can readily compete. Those occurring within the protein lead to the sequestration of some iron, but this is likely to be located at various sites on the protein, including the protein channels. Thus, the effective iron capacity would be expected to be dependent on how iron is added. For the same total amount of iron, more should be taken up if added in a single addition rather than a series of smaller ones because autoxidation processes lead to a gradual blockage of the channels, preventing iron from later additions from accessing the cavity. This proposal is further supported by the data for E127Q and H130E EcBFRs, which showed that iron core formation rates are linked to effective iron capacities.

Studies of the ferroxidase center variant E18A EcBFR showed that core formation is severely restricted when the ferroxidase center is disabled. A similar result was obtained by pretreating wild-type BFR with enough zinc(II) to effectively block all of the ferroxidase centers. These data are in direct contrast to studies of core formation in wild-type and mutant HuHF (*19*), which showed that, at low iron loadings, iron(II) oxidation proceeds via the ferroxidase center only, while at high iron(II) loadings, oxidation at the core surface becomes the dominant mechanism. In the absence of a functional ferroxidase center, initial core formation (nucleation) in HuHF was slow but became significantly more rapid following subsequent iron additions, i.e., rates of core formation at least partially recovered. Thus core formation in EcBFR and mammalian ferritins are distinct processes: EcBFR lacking a functional ferroxidase center cannot support significant core formation, whereas similarly deficient human ferritin can.

What is the role of the ferroxidase center in EcBFR core formation? One possibility is that the ferroxidase center is required only for the nucleation of the core, after which the core surface becomes the site of catalysis. In the absence of a ferroxidase center, core nucleation may not be able to occur in such a way that can subsequently support catalysis of iron(II) oxidation. Alternatively, the ferroxidase center may be catalytically functional throughout the core formation process, such that disabling of the center significantly inhibits further core formation. These possibilities were investigated by adding zinc(II) to BFR containing a substantial core followed by the addition of iron(II) (Figure 6), which revealed that even under these conditions, zinc(II) was able to inhibit core formation. Zinc(II) inhibition of core formation has also been reported for ferritin containing an established iron core (*38*), though in that case, the effect was interpreted and modeled in terms of zinc blocking iron(II)-binding sites on the surface of the core, consistent with the high excess of zinc(II) over protein and the approximate 1:1 ratio of zinc(II) to iron(II) added. In the experiments reported here, much lower amounts of zinc(II) were used, and it is extremely unlikely that the proportion of the core surface binding sites that could be blocked by, e.g., 12 zinc(II) ions per EcBFR could account for the dramatic effect observed. It is also significant that, in relative terms, the effect of zinc(II) on cores of 800 and 1200 irons was essentially identical, indicating that the effect of zinc(II) is independent of the core surface area. One way in which zinc(II) could exert such an effect would be through binding in the channels connecting the protein cavity with the bulk medium. This would prevent iron(II) from entering the cavity. Experiments with copper(II) to enhance core formation rates were carried out to address this question. These showed that further core formation in wild-type and in E18A EcBFR loaded with iron in the presence of copper(II) (which restored the ability of the protein to form a sizable core) could not be inhibited by zinc(II) (Figures 7 and 8). Thus, zinc(II) does not appear to inhibit iron(II) access to the cavity. All of these data combined lead to the conclusion that the ferroxidase center is catalytically active throughout core formation, not just during core nucleation, and that zinc(II) inhibition of core formation is mediated by its binding at the ferroxidase center. Copper(II), which provides an alternative catalytic site for iron(II) oxidation independent of the ferroxidase center (*23*), obviates the inhibitory effect of zinc(II).

What is the mechanism by which the ferroxidase center maintains its activity throughout core formation? We have previously proposed a number of possible mechanisms for core formation ranging from the linked-transfer model, in which the ferroxidase center is itself stable but is capable of catalyzing further iron(II) oxidation, to the sequential transfer model, in which the ferroxidase center cycles by filling with

iron(II), oxidizing the iron, and empyting the iron(III) product into the cavity (*7*). The recent X-ray structures of the BFR from the anaerobe *Desulfovibrio desulfuricans* are the first structures of BFR to be solved with iron(III) at the ferroxidase center, and they show that the two iron(III) ions at each center are bridged in the manner suggested by spectroscopy and required for formation of a stable center (*39*). There are important mechanistic differences between BFR and H-chain ferroxidase centers. First, the BFR center does not empty of iron following phase 2 iron(II) oxidation and the phase 2 reaction cannot be regenerated in BFR containing 48 iron(III)/molecule, as it can be in mammalian H-chain ferritin (*12*, *18*, *21*, *40*). Second, the iron:oxygen stoichiometry for the EcBFR phase 2 reaction is 4:1, whereas it is 2:1 for H-chain ferritin (*17*, *18*, *21*, *41*). Such differences are a likely result of the structural differences between the centers (*6*, *39*, *42*). One of the ferroxidase center ligands in HuHF, Glu61, can adopt an alternative position in which it faces the internal cavity. It is proposed that, following iron(II) oxidation at the ferroxidase center, Glu61 swings away from the center toward the cavity and is thus important for core nucleation. This provides a possible explanation for why the diferric form of the center of HuHF is labile. Glu61 is not conserved in EcBFR, which has H130 at the structurally equivalent position, consistent with the observed stability of the diferric ferroxidase center in EcBFR. On the basis of the data presented here and previous work on EcBFR, we propose the following mechanism for core formation, in which the ferroxidase center plays a central role.

Following completion of the phase 2 reaction, μ-oxo-bridged ferric ion dimers most likely occupy the 24 ferroxidase centers of BFR (*21*). Further added iron(II) accesses the protein cavity via the channels running through the protein coat (*1*, *39*). Regions of the inner surface of the protein coat are negatively charged (e.g., residues Glu47, Asp50, and Asp126) and iron(II) ions entering the empty cavity are likely to bind at these nucleation sites. Iron(II) ions entering a cavity already containing a core bind at the growing core surface. Upon binding the acidic residues and/or growing core surface, iron(II) becomes oxidized to iron(III):

$$4Fe^{2+} \rightarrow 4Fe^{3+} + 4e^{-} \quad (1)$$

The oxidized iron at the protein or core surface subsequently undergoes a hydrolysis reaction:

$$4Fe^{3+} + 8H_2O \rightarrow 4[FeOOH] + 12H^{+} \quad (2)$$

and the sum of reactions 1 and 2 is

$$4Fe^{2+} + 8H_2O \rightarrow 4[FeOOH] + 12H^{+} + 4e^{-} \quad (3)$$

The electrons resulting from iron(II) oxidation are channelled to the ferroxidase center. In thermodynamic terms, this is a favorable reaction because the redox potential of iron at the ferroxidase center is believed to be ~0 mV (*43*), while that of iron in the core is much lower: ~−400 mV for the phosphate-rich core of *Azotobacter vinelandii* BFR (*8*) and −190 to −415 mV (over the pH range 7−9) for horse spleen ferritin (*44*). Therefore, core iron is reducing relative to the ferroxidase center iron. In terms of kinetics, this process is reasonable: in the case of the empty cavity, the acidic residues that are proposed to be the site of initial iron binding are all within 10 Å of the ferroxidase center and are, therefore, well within range for rapid electron transfer (*45*). In the case of iron(II) binding at the core surface, the existing core acts as a molecular wire for electron transfer to the ferroxidase center. The binding of an iron(II) ion at the iron(III) core surface generates a species that may be considered analogous to smaller polynuclear (e.g., trinuclear) iron mixed-valence species. Studies of such species have shown that they are valence-delocalized at room temperature, i.e., they undergo rapid intramolecular electron transfer (*46*). Transfer of electrons from iron(II) ions at the core surface into the existing core has been reported previously in a study of the effect of phosphate on iron interactions with both mammalian ferritin and BFR (*9*, *47*). Electrons arriving at the ferroxidase center cause the reduction of the μ-oxo-bridged diferric species to a diferrous center once more:

$$2[Fe(III)_2O{-}P]^{z} + 4e^{-} + 4H^{+} \rightarrow 2[Fe(II)_2{-}P]^{z} + 2H_2O \quad (4)$$

where z represents the charge on the protein. We note that this would most likely involve ligand rearrangement resulting in the loss of the μ-oxo bridge between the irons. The reduced ferroxidase center is then able to react with an oxidant, which we have previously shown can be dioxygen or hydrogen peroxide (*21*, *48*):

$$[Fe(II)_2{-}P]^{z} + O_2 + H_2O \rightarrow [Fe(III)_2O{-}P]^{z} + H_2O_2 \quad (5)$$

$$[Fe(II)_2{-}P]^{z} + H_2O_2 \rightarrow [Fe(III)_2O{-}P]^{z} + H_2O \quad (6)$$

where the sum of reactions 5 and 6 is

$$2[Fe(II)_2{-}P]^{z} + O_2 \rightarrow 2[Fe(III)_2O{-}P]^{z} \quad (7)$$

The overall core formation reaction is thus the sum of reactions 3, 4, and 7, i.e., reaction 8:

$$4Fe^{2+} + O_2 + 6H_2O \rightarrow 4[FeOOH] + 8H^{+} \quad (8)$$

This mechanism accounts for the dependence of core formation on a functional ferroxidase center and on the surface area of the growing core. The latter is the site of iron(II) oxidation (but not dioxygen reduction) and so the rate of core formation depends on the concentration of binding sites. The mechanism also accounts for zinc(II) inhibition of core formation since zinc(II) displaces iron(II) but not iron(III) from the ferroxidase center. Given the observed pH dependence of BFR core formation, clearly, the rate-determining step involves a reaction in which protons are released. Thus the hydrolysis reaction (eq 2) is very likely the rate-determining step, but this may be coupled to the reduction of iron(III) at the ferroxidase center (eq 4), which involves the uptake of protons.

The results may provide some insight into why all the EcBFR subunits contain a ferroxidase center; since they are required for catalysis of core formation, an advantage is gained if all subunits have one. The ability of the core surface of mammalian ferritins to catalyze further core formation means that the ferroxidase centers are not essential for core formation beyond the stage of core nucleation, and thus heteropolymers of H- and L-chain ferritins, the latter lacking intrasubunit ferroxidase centers of the type illustrated in Figure 1, are common. This raises the intriguing question

of why the EcBFR core surface alone is apparently not capable of catalyzing further core formation. Our mechanistic proposals suggest that the core surface is capable of catalyzing iron(II) oxidation but not dioxygen reduction. Therefore, one possibility is that dioxygen cannot readily gain access to the core. We note that both 3- and 4-fold channels through the EcBFR coat are hydrophilic (*6*), whereas the 4-fold channels in mammalian ferritins are largely hydrophobic (*1* and references therein). These could act as the access route for dioxygen in mammalian ferritins since dioxygen is nonpolar. This possibility is consistent with our observation that the ferroxidase center variant E18A EcBFR, and Zn(II)-EcBFR, protects iron(II) against oxidation relative to protein free controls.

ACKNOWLEDGMENT

We thank BBSRC for supporting our work on bacterioferritin; JIF for equipment; Christine Moore, Nick Cull, and Dave Clarke for preparation of bacterioferritin samples; and Professor Denny Chasteen for valuable discussions. S.B. thanks her family for financial support.

REFERENCES

1. Harrison, P. M., and Arosio, P. (1996) *Biochim. Biophys. Acta 1275*, 161−203.
2. Andrews, S. C. (1998) *Adv. Microb. Physiol. 40*, 281−351.
3. Chasteen, N. D., and Harrison, P. M. (1999) *J. Struct. Biol. 126*, 182−194.
4. Chasteen, N. D. (1998) *Met. Ions Biol. Syst. 35*, 479−514.
5. Carrondo, M. A. (2003) *EMBO J. 22*, 1959−1968.
6. Frolow, F., Kalb, A. J., and Yariv, J. (1994) *Nat. Struct. Biol. 1*, 453−460.
7. Le Brun, N. E., Thomson, A. J., and Moore, G. R. (1997) *Struct. Bonding 88*, 103−138.
8. Watt, G. D., Frankel, R. B., Papaefthmiou, G. C., Spartalian, K., and Stiefel, E. I. (1986) *Biochemistry 25*, 4330−4336.
9. Watt, G. D., Frankel, R. B., Jacobs, D., Huang, H., and Papaefthymiou, G. C. (1992) *Biochemistry 31*, 5672−5679.
10. Stiefel, E. I., and Watt, G. D. (1979) *Nature 279*, 81−83.
11. Andrews, S. C., Le Brun, N. E., Barynin, V., Thomson, A. J., Moore, G. R., Guest, J. R., and Harrison, P. M. (1995) *J. Biol. Chem. 270*, 23268−23274.
12. Le Brun, N. E., Wilson, M. T., Andrews, S. C., Harrison, P. M., Guest, J. R., Thomson, A. J., and Moore, G. R. (1993) *FEBS Lett. 333*, 197−202.
13. Le Brun, N. E., Andrews, S. C., Guest, J. R., Harrison, P. M., Moore, G. R., and Thomson, A. J. (1995) *Biochem. J. 312*, 385−392.
14. Guex, M., and Peitsch, M. C. (1997) *Electrophoresis 18*, 2714−2723 and http://www.expasy.org/spdbv/.
15. Macara, I. G., Hoy, T. G., and Harrison, P. M. (1972) *Biochem. J. 126*, 151−162.
16. Macara, I. G., Hoy, T. G., and Harrison, P. M. (1973) *Biochem. J. 135*, 343−348.
17. Xu, B., and Chasteen, N. D. (1991) *J. Biol. Chem. 266*, 19965−19970.
18. Yang, X., Chen-Barrett, Y., Arosio, P., and Chasteen, N. D. (1998) *Biochemistry 37*, 9743−9750.
19. Zhao, G., Bou-Abdallah, F., Arosio, P., Levi, S., Janus-Chandler, C., and Chasteen, N. D. (2003) *Biochemistry 42*, 3142−3150.
20. Le Brun, N. E., Keech, A. M., Mauk, M. R., Mauk, A. G., Andrews, S. C., Thomson, A. J., and Moore, G. R. (1996) *FEBS Lett. 397*, 159−163.
21. Yang, X., Le Brun, N. E., Thomson, A. J., Moore, G. R., and Chasteen, N. D. (2000) *Biochemistry 39*, 4915−4923.
22. Hutchings, M. I., Shearer, N., Wastell, S., Van Spanning, R. J. M., and Spiro, S. (2000) *J. Bacteriol. 182*, 6434−6439.
23. Baaghil, S., Thomson, A. J., Moore, G. R., and Le Brun, N. E. (2002) *J. Chem. Soc., Dalton Trans.*, 811−818.
24. Stookey, L. L. (1970) *Anal. Chem. 42*, 779−781.
25. Smith, P. K., Krohn, R. I., Hermanson, G. T., Mallia, A. K., Gartner, F. H., Provenzano, M. D., Fujimoto, E. K., Goeke, N. M., Olson, B. J., and Klenk, D. C. (1985) *Anal. Biochem. 150*, 76−85.
26. Falk, J. E. (1964) in *Porphyrins and Metalloporphyrins*, BBA Library Vol. 2, pp 181−182, Elsevier North-Holland, Amsterdam.
27. Bauminger, E. R., Harrison, P. M., Hechel, D., Nowik, I., and Treffry, A. (1991) *Biochim. Biophys. Acta 1118*, 48−58.
28. Laemmli, U. K. (1970) *Nature 227*, 680−685.
29. Mann, S., Williams, J. M., Treffry, A., and Harrison, P. M. (1987) *J. Mol. Biol. 198*, 405−416.
30. Ford, G. C., Harrison, P. M., Rice, D. W., Smith, J. M. A., Treffry, A., White, J. L., and Yariv, J. (1984) *Philos. Trans. R. Soc. London B304*, 551−565.
31. Powell, A. K. (1997) *Struct. Bonding 88*, 1−38.
32. Harrison, P. M., Fischbach, F. A., Hoy, T. G., and Haggis, G. H. (1967) *Nature 216*, 1188−1190.
33. Mann, S., Bannister, J. V., and Williams, R. J. P. (1986) *J. Mol. Biol. 188*, 225−232.
34. Massover, W. H., and Cowley, J. M. (1973) *Proc. Natl. Acad. Sci. U. S. A. 70*, 3847−3851.
35. Lindsay, S., Brosnahan, D., Lowery, T. J., Crawford, K., and Watt, G. D. (2003) *Biochim. Biophys. Acta 1621*, 57−66.
36. Yablonski, M. J., and Theil, E. C. (1992) *Biochemistry 31*, 9680−9684.
37. Treffry, A., Bauminger, E. R., Hechel, D., Hodson, N. W., Nowik, I., Yewdall, S. J., and Harrison, P. M. (1993) *Biochem. J. 296*, 721−728.
38. Macara, I. G., Hoy, T. G., and Harrison, P. M. (1973) *Biochem. Soc. Trans.* 102−104.
39. Macedo, S., Romão, C. V., Mitchell, E., Matias, P. M., Liu, M. Y., Xavier, A. V., LeGall, J., Teixeira, M., Lindley, P., and Carrondo, M. A. (2003) *Nat. Struct. Biol. 10*, 285−290.
40. Treffry, A., Hirzmann, J., Yewdall, S. J., and Harrison, P. M. (1992) *FEBS Lett. 302*, 108−112.
41. Sun, S., Arosio, P., Levi, S., and Chasteen, N. D. (1993) *Biochemistry 32*, 9362−9369.
42. Lawson, D. M., Artymuik, P. J., Yewdall, S. J., Smith, J. M. A., Livingstone, J. C., Treffry, A., Luzzago, A., Levi, S., Arosio, P., Cesareni, G., Thomas, C. D., Shaw, W. V., and Harrison, P. M. (1991) *Nature 349*, 541−544.
43. Le Brun, N. E., Cheesman, M. R., Thomson, A. J., Moore, G. R., Andrews, S. C., Guest, J. R., and Harrison, P. M. (1993) *FEBS Lett. 323*, 261−266.
44. Watt, G. D., Frankel, R. B., and Papaefthmiou, G. C. (1985) *Proc. Natl. Acad. Sci. U. S. A. 82*, 3640−3643.
45. Page, C. C., Moser, C. C., Chen, X., and Dutton, P. L. (1999) *Nature 402*, 47−52.
46. Wu, C. C., Hunt, S. A., Gantzel, P. K., Gutlich, P., and Hendrickson, D. N. (1997) *Inorg. Chem. 36*, 4717−4733.
47. Jacobs, D., Watt, G. D., Frankel, R. B., and Papaefthymiou, G. C. (1989) *Biochemistry 28*, 9216−9221.
48. Bou-Abdallah, F., Lewin, A. C., Le Brun, N. E., Moore, G. R., and Chasteen, N. D. (2002) *J. Biol. Chem. 277*, 37064−37069.

BI035253U